AAPPS Bulletin

REVIEW ARTICLE

Open Access

Yemilab, a new underground laboratory in Korea

Yeongduk Kim[1,2] and Hyun Su Lee[1,2*]

Abstract

In September 2022, Yemilab, a new underground laboratory, was finally completed in Jeongseon, Gangwon Province, South Korea. Situated at a depth of 1000 m, it boasts an exclusive experimental area of 3000 m^2. Currently, preparations are in progress for the AMoRE-II experiment, which aims to investigate neutrinoless double beta decay, as well as for the COSINE-100 upgrade (COSINE-100U), a direct dark matter detection experiment. Both experiments are scheduled to commence in the second quarter of 2024 at Yemilab. Furthermore, the facility encompasses a cylindrical pit, approximately 6300 m^3 in volume, designed to serve as a multipurpose laboratory. This laboratory will facilitate next-generation experiments focusing on neutrinos, dark matter, and related areas of research. This article presents a detailed overview of Yemilab's construction, infrastructure, and its pivotal physics programs.

Keywords Underground laboratory, Dark matter, Neutrino

1 Introduction

The discovery of the Higgs boson in 2012 [1, 2] marked the identification of the last fundamental particle predicted by the Standard Model within the framework of quantum field theory. This model integrates 12 elementary particles and their interactions, alongside 4 mediator particles and the Higgs boson, which imparts mass to the elementary particles [3]. Despite these advancements, critical questions about the inherent nature of these particles and their interactions remain unanswered, i.e., inquiries into the reasons behind the minuscule mass of neutrinos, one of the fundamental particles [4]. Moreover, observations in astronomy since the establishment of the Standard Model suggest the existence of additional mass in the universe beyond observable objects and materials [5, 6]. These observations also hint at an unknown form of energy driving the acceleration of the universe's expansion [5, 7, 8], though their exact nature remains unidentified [3].

Observational evidence strongly suggests that dark matter comprises particles not yet accounted for in the Standard Model, hypothesized to interact very weakly, if at all, with known particles or matter [9]. Despite extensive theoretical speculation, experimental searches since the 1980s have yet to confirm their existence [10, 11]. The discovery of neutrino oscillations through solar [12], atmospheric [13], reactor [14], and accelerator neutrinos [15, 16] has confirmed that neutrinos possess a very small, but nonzero, mass [3]. This revelation challenges our understanding of mass generation via the Higgs boson and raises the possibility of the existence of heavier right-handed neutrinos as a plausible explanation for the small neutrino mass [17, 18].

The Standard Model, therefore, remains incomplete, failing to account for phenomena confirmed by experimental evidence, such as the mass of neutrinos, dark matter, and dark energy. Various facilities in Asia have been developed to study these fundamental aspects of physics [19–22].

On the sea level laboratories, the atmosphere's high-energy cosmic rays generate many particles, creating

*Correspondence:
Hyun Su Lee
hyunsulee@ibs.re.kr
[1] Center for Underground Physics, Institute for Basic Science, Daejeon 34126, Republic of Korea
[2] University of Science and Technology, Daejeon 34113, Republic of Korea

background radiation that obscures the measurement of rare neutrino signals or the detection of dark matter interactions. Consequently, experiments conducted in deep underground laboratories, beyond the reach of particles generated by cosmic rays, become crucial. Over the past five decades, numerous deep underground laboratories worldwide have emerged as national research institutes, playing a pivotal role in dark matter and neutrino physics [23, 24].

In Korea, the Yangyang Underground Laboratory (Y2L) [25] initiated valuable research on dark matter [26, 27] and neutrino physics [28, 29]. However, due to its limited experimental space and depth compared to world-leading underground laboratories such as SURF (US), SNOLAB (Canada), Boulby (UK), Jingping (China), Kamioka (Japan), and LNGS (Italy) [23, 24], the need for a new underground laboratory to support future world-leading experiments became apparent. This need led to the recent construction of Yemilab [30], which signifies a significant advancement in the field of neutrino and dark matter research. In this report, we will review the physics and projects conducted at Y2L as well as those being executed at Yemilab.

2 Yemilab construction

Since 2013, the Center for Underground Physics (CUP) at the Institute for Basic Science (IBS) in Korea has planned the construction of a new underground laboratory to augment the existing facilities at Y2L, which has a limited experimental space of approximately 200 m^2 at a depth of around 700 m. In the search for a suitable location that would allow for a laboratory deeper than 1000 m, several candidate sites were considered, taking into account the length of the underground tunnel and the depth of the laboratory. After about 3 years of comprehensive investigation, Mt. Yemi, with a peak height of 989 m and encompassing the SM Handuk Iron Mine Co., Ltd (Handuk) in Jeongseon-gun, was selected (see Fig. 1). An active mine was chosen for its existing infrastructure, including a 600-m vertical shaft with a 6-m diameter, which offered cost savings for tunnel and laboratory excavation. Another advantage of the Mt. Yemi site was its utilization of the operational Handuk mine, allowing construction to proceed without environmental damage and without significant legal or permitting obstacles [30].

By the end of 2016, approximately $17 million in funding was secured for the first construction phase, which included the installation of the human-riding cage and the excavation of the primary tunnel. The installation of the cage was completed in December 2018, and the first phase concluded with the tunnel construction in August 2020. Early in 2021, an additional $8 million in funding was secured for the second phase, with work resuming at the end that year. This phase involved excavating a pit to house a 6300-m_3 Liquid Scintillation Counter (LSC) and installing essential facilities such as electricity, ventilation, communication, and fire safety facilities for the underground laboratory. The second construction phase was completed in August 2022, establishing the basic framework of Yemilab, as one can see in Fig. 2.

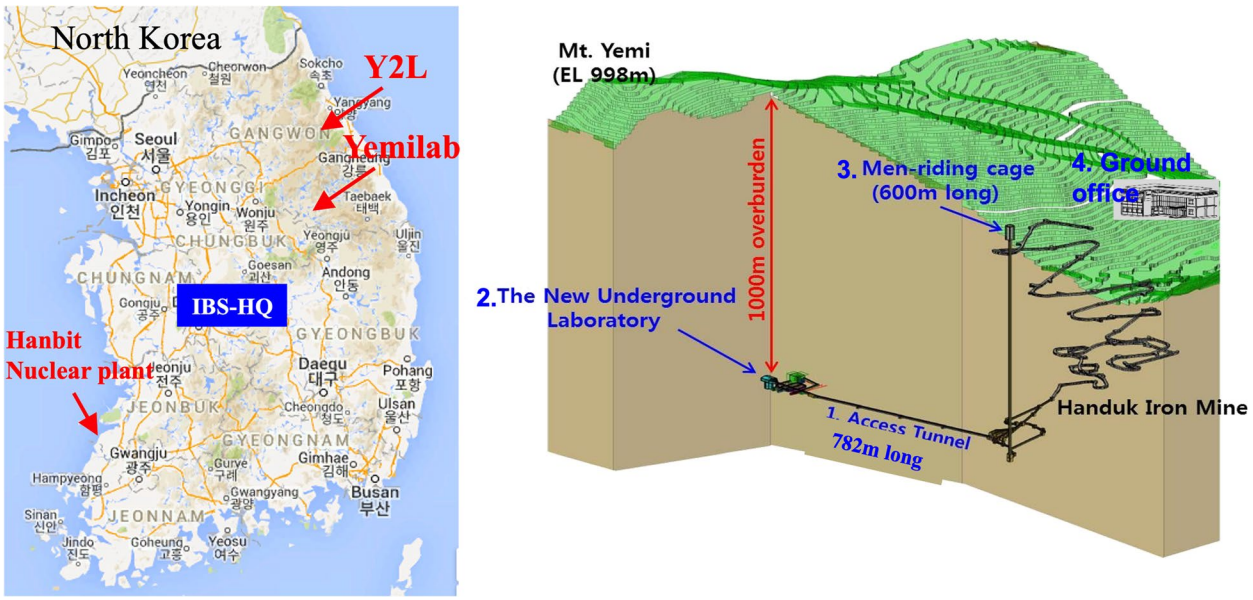

Fig. 1 (Left) Location of Yemilab in Korea. (Right) Structure of Yemilab, featuring an entrance through a vertical shaft connected to an approximately 780-m-long entrance tunnel

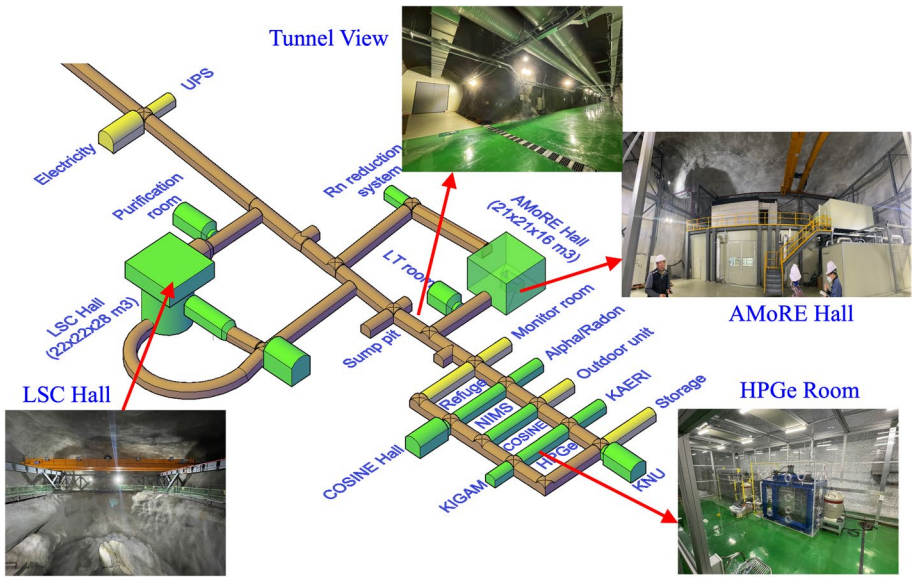

Fig. 2 The floor plan of Yemilab's experimental area

With the completion of Yemilab's fundamental structure, interior enhancements were undertaken in 2023, including the installation of cranes, vehicle washing systems, dustproof doors, and floor and wall coatings. These improvements provided Yemilab with the necessary infrastructure to begin experiments. Starting in September 2023, the relocation of various facilities from Y2L to Yemilab commenced. By the end of 2024, once all relocations are finalized, each experiment will embark on a new phase at Yemilab [30].

The entry point of the Yemilab tunnel, situated at an elevation of − 35 m in the Handuk area, reaches a depth of 604 m. The access tunnel, excavated with a cross-section of 5 m in both width and height, features a 12 % downward slope over its 782 m length to achieve a depth increase of approximately 100 m. To accommodate the rotation of large construction vehicles, turning shelters were placed every 90 m, with six in total along the access tunnel; four of these shelters are adaptable for experimental use. At the tunnel's end, a horizontal section was carved out to create the experimental area, comprising 23 independent spaces: 16 for experiments or related equipment and seven for operational support.

Focusing only on the experimental spaces, the largest laboratory is the LSC Hall, featuring a 22-m square dome above a 20-m-diameter, 20-m-deep cylindrical pit, resulting in a 6300-m^3 volume designed for versatile detector applications. The next largest, the AMoRE Hall, measures 21 m (width) by 21 m (length) by 16 m (height). Other spaces include one measuring 12 m (width) by 17 m (length) by 10 m (height), three at 8 m (width) by 15 m (length) by 8 m (height), and two at 7 m (width) by 25 m (length) by 7 m (height), with the remaining areas adhering to the standard 5 m by 5 m cross-section. Figure 2 illustrates Yemilab's layout.

Yemilab's electrical infrastructure supports a 1600 kW (2000 KVA) capacity, allocating approximately 200 kW for operational needs like lighting and ventilation, leaving 1400 kW for experimental demands. A 260 kW uninterrupted power supply (UPS) unit and an emergency surface generator, which can deliver an immediate 360 kW, ensure continuous operation during power outages [30].

Ventilation within Yemilab is efficiently managed through a 1-m-diameter duct that draws air from the vertical shaft, distributing 39,000 m^3/h throughout Yemilab. Of this, 12,000 m^3/h is allocated to the outdoor unit room of the experimental area's air conditioning systems, maintaining temperatures below 40 $^{\circ}$C with an assumed heat load of 100 kW. The remaining 27,000 m^3/h is circulated through the experimental spaces, enabling roughly ten air exchanges daily and maintaining a 26 $^{\circ}$C environment with radon levels under 50 Bq/m^3.

During the summer season, usually from June to September, the facility faces challenges with increased radon concentrations, which can surge to approximately 2000 Bq/m^3. This spike is attributed to the elevated surface temperatures and the consequent significant slowdown in natural ventilation within the mine. To counteract this, the installation of a radonless air system is underway. This system aims to maintain radon levels below 150 Bq/m$Â^3$ by directly supplying surface air into the underground spaces.

Post-epoxy floor coating, the PM10 dust level is below 10 μg/m^3, surpassing the Korean office environment standard of 50 μg/m^3. After relocation of Y2L to Yemilab, stricter controls aim to reduce this further to under 5 μg/m^3. Yemilab's Radon Reduction System (RRS) ensures air with less than 100 mBq/m^3 radon with a capacity of 50 m^3/h, suitable for sensitive experiments and approximating a Class 1,000 cleanroom. An additional 250 m^3/h capacity RRS is slated for installation in 2025 [30].

Muon flux measurements, conducted with the AMoRE-II muon veto system, revealed a preliminary flux of 1.0×10^{-7}μ/cm^2/s at Yemilab, four times lower than the muon flux at Y2L of 3.8×10^{-7}μ/cm^2/s [31] and aligning with an expection based on GEANT4 simulation of 8.2×10^{-8}μ/cm^2/s [32].

The neutron flux at Yemilab was measured at three locations using multiple Bonner spheres with He-3 detectors. The thermal neutron flux was found to be $(1.9 \pm 0.1) \times 10^{-5}/cm^2/s$, and the fast neutron (1–10 MeV) flux was $(1.4 \pm 0.1) \times 10^{-5}/cm^2/s$. These values are comparable to those at Y2L, where the thermal and fast neutron fluxes were $(1.4 - 2.4) \times 10^{-5}/cm^2/s$ and $(0.4 - 0.7) \times 10^{-5}/cm^2/s$ respectively. Gamma background measurements were conducted at several locations using a 3″ NaI detector and a HPGe detector without shielding, and comparisons with simulations are ongoing.

3 AMoRE——a neutrinoless double beta decay experiment

3.1 AMoRE overview

Neutrinos were confirmed to possess mass through oscillation experiments involving solar and atmospheric neutrinos [13, 33]. The three mixing angles and mass differences between the neutrino types have been measured, thanks to additional data from reactor and accelerator oscillation experiments [14–16]. Although the absolute masses of neutrinos remain unknown, we understand that they are significantly smaller than the mass of the electron, the lightest known massive particle. This understanding is supported by constraints from beta decay experiments [34] and cosmological observations [5].

The minuscule mass of neutrinos and the non-observation of right-handed neutrinos present challenges to the hypothesis that neutrinos are Dirac particles, similar to other charged leptons. Alternatively, the seesaw mechanism proposes that the small active neutrino masses arise from the existence of heavy right-handed sterile neutrinos [17, 18]. Typically, this mechanism implies that neutrinos are Majorana particles, meaning they are their own antiparticles, which would result in the violation of lepton number conservation [35].

Experimentally distinguishing between Dirac and Majorana neutrinos is challenging. The most direct method proposed is the detection of neutrinoless double beta ($0\nu\beta\beta$) decay [36]. The observation of this decay would not only confirm the Majorana nature of neutrinos but also indicate that the neutrino mass includes a Majorana mass term [37].

An unresolved question in physics is why the universe is dominated by matter over antimatter. A hypothesis within the neutrino sector, known as leptogenesis [38, 39], suggests a possible explanation. The realization of this matter-antimatter asymmetry through leptogenesis typically requires neutrinos to be Majorana particles. Thus, detecting $0\nu\beta\beta$ decay is considered a crucial step towards confirming the Majorana nature of neutrinos and addressing this cosmic imbalance [4, 40].

Considering only the light neutrino exchange contribution to $0\nu\beta\beta$ decay, a half life of $0\nu\beta\beta$, $T^{0\nu}_{1/2}$, has related,

$$\frac{1}{T^{0\nu}_{1/2}} = G_{01} \left| M^{0\nu}_{\text{light}} \right|^2 \frac{m^2_{\beta\beta}}{m^2_e}, \qquad m_{\beta\beta} = \left| \sum_{i=1}^{3} |U^2_{\text{ei}}|\, e^{i\varphi_{\text{i}}}\, m_{\text{i}} \right|, \tag{1}$$

where G_{01} and $M^{0\nu}_{\text{light}}$ are the phase space and nuclear matrix element (NME) specific to light neutrino exchange, respectively, and $m_{\beta\beta}$ is the effective Majorana mass. U_{ei} is the Pontecorvo-Maki-Nakagawa-Sakata (PMNS) matrix components for mixing between ith mass eigenstate and electron flavor eigenstate [41] and the φ_{i} are Majorana phases which cannot be probed by oscillation experiments.

The effective Majorana mass parameter depends on the mass hierarchy of neutrinos whether it is normal or inverted ordering. It is possible for this parameter to be zero in the case of normal hierarchy, due to destructive interference between the Majorana phases. Recent long-baseline neutrino oscillation experiments have shown a preference for normal mass ordering [42, 43]. Future experiments are expected to provide more precise measurements of neutrino mass ordering [44–46]. Discovering $0\nu\beta\beta$ decay would confirm lepton number violation and help determine the absolute neutrino mass scale, shedding light on fundamental questions about the universe's matter-antimatter asymmetry and its cosmological implications.

The AMoRE experiment aims to detect $0\nu\beta\beta$ decay in ^{100}Mo nuclei using molybdate-based crystals at millikelvin temperatures [47]. The Q-value for the ^{100}Mo double-beta decay is 3034.40 ± 0.17 keV [48]. The experiment strives for a zero background in the region of interest (ROI, 3034 ± 10 keV) to ensure that background counts are minimal over a 5-year operation.

The AMoRE project progresses in phases. With AMoRE-I completed in 2023, preparations are underway for AMoRE-II as shown in Table 1. Each detector module in the AMoRE experiment consists of a molybdate scintillating crystal, whose size varies 4–6 cm diameter and height, accompanied by a pair of phonon and photon sensors that include a metallic magnetic calorimeter (MMC) for temperature measurement. This dual-signal detection method allows for effective discrimination between α background and β/γ events [49].

When a scintillating crystal absorbs energy, it experiences a rise in temperature. This temperature increase is measured using a metallic magnetic calorimeter (MMC) and a superconducting quantum interference device (SQUID) which is connected to a gold film (phonon collector) deposited on the crystal as shown in Fig. 3. To detect scintillation photons emitted by the crystal, a light detector comprising either a Si or Ge wafer, along with another MMC+SQUIOD sensor, is utilized. Figure 3 illustrates the design common to all AMoRE detector modules. In this design, a crystal is secured using PTFE clamps within a structure made of low-background copper. This copper frame functions both as a conduit for cooling the crystals and sensors and as a thermal bath for the entire detector module. Positioned at the bottom of the module, the MMC sensor for the phonon channel is critical for the operation. The bottom surface of the crystal is coated with a vapor-deposited gold film, serving as a phonon collector. About twenty annealed gold wires establish a thermal linkage between this phonon-collector film and the MMC sensor. Additionally, another gold wire connects the MMC sensor to the copper holder, ensuring a thermal pathway to the heat bath. At low temperatures, the heat capacity of the MMC sensor is the predominant factor for the entire detector module [50]. To enhance the efficiency of scintillation photon collection, the crystal is surrounded by light-reflection foils (Vikuiti), chosen for their high reflectivity.

The CUPID-Mo experiment, another project focusing on Mo-100 double beta decay, uses NTD (neutron transmutation doped) sensors to read LMO crystals. These sensors offer the advantage of simple electronics for resistance measurement, but they are limited by slow timing, with a rise time of about 20 ms. The most significant background source for CUPID-Mo is intrinsic pile-up from $2\nu\beta\beta$ decay due to this slow timing. In contrast, the MMC sensors used in the AMoRE-II experiment have faster timing, around 3 ms, making pile-up background less critical.

Table 1 The phases of AMoRE project

	AMoRE-I	AMoRE-II
Mass (kg)	6.2	160
Background (ckky)	3×10^{-3}	10^{-4}
$T^{0\nu}_{1/2}$ sensitivity (years)	3.6×10^{24}	5.6×10^{26}
$m_{\beta\beta}$ sensitivity (meV)	70-140	17-30
Schedule	2019–2023	2025–2030

3.2 AMoRE-I

AMoRE-I ran steadily at the 700-m-deep Y2L from 2019 to 2023. The AMoRE-I detector consists of a 6.2 kg array comprising thirteen $^{48depl}Ca^{100}MoO_4$ (CMO) crystals and five $Li_2{}^{100}MoO_4$ (LMO) crystals, corresponding to 3.0 kg of ^{100}Mo. The objective of AMoRE-I is to confirm the long-term stability of the detectors and provide background data for the subsequent phase of the

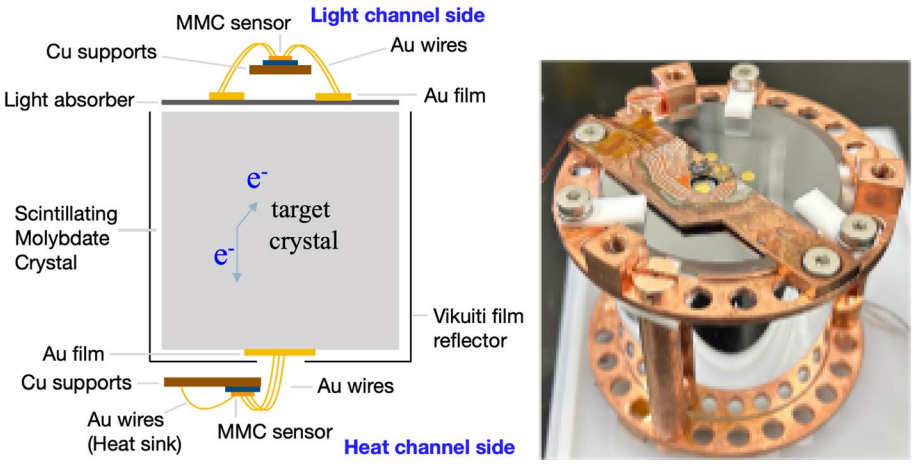

Fig. 3 Schematic of the AMoRE detector system (left) and a detector module used in AMoRE-II (right), comprising a ^{100}*Mo*-enriched crystal, a photon detector, and a phonon detector. Figures adapted from Ref. [51]

AMoRE experiment. For the CMO crystals, it is necessary to deplete the ^{48}Ca isotopes since the Q-value of ^{48}C double-beta decay is 4.27 MeV, which contributes significantly to the background at the ROI for the ^{100}Mo experiment. Based on the results obtained in our previous pilot study with a 111 kg.day exposure using CMO crystals, we achieved a background rate of 0.55 count/keV/kg/year (ckky) in the energy range of 2850–3150 keV [28, 52].

As we aim to maintain stable operation of AMoRE-I for long-term data collection, we set the temperature of the detector tower slightly above 10 mK. The cryogenic system, equipped with a dilution refrigerator, has a cooling power of 1.3 μW at 12 mK. We adjusted the cooling power within the control budget to ensure stability throughout the year-long operation, thereby mitigating any instabilities arising from fridge operations or utility supplies.

Additionally, we implemented a two-stage temperature control system using a dummy MMC channel operating in sensitive thermometer mode [53]. This temperature control mechanism can maintain the temperature of the detector tower within an root-mean-square (RMS) fluctuation of 0.5 μK. Following the completion of the commissioning periods, we have maintained the detector tower at 12 mK during science runs for long-term data collection.

Figure 4a and b show the ratio of light signal to heat signal as a function of energy derived from the heat signal for a CMO and an LMO crystal, respectively. The light signals from the alpha background form the lower horizontal bands at the high energy sides, with the LMO crystal exhibiting significantly less alpha contamination compared to CMO crystal. However, the LMO crystal exhibits reduced discrimination capabilities between β/γ and α particles, a consequence of its lower scintillation yield. We select single-hit events in the β/γ band, which were vetoed by the muon detector signal that surround the shields. The background level around Q-value was found approximately 0.03 ckky, marking an order of magnitude improvement over the results from the previous pilot experiment [28]. The total exposure was about 3.9 kg.day. The expected discovery sensitivity for $0\nu\beta\beta$ decay is $T^{0\nu}_{1/2} > 3.0 \times 10^{24}$ years at a 90% confidence level as shown in Fig. 7. Consequently, we anticipate that the data from AMoRE-I will set a more stringent limit than the current best limit for ^{100}Mo, achieved by the CUPID-Mo experiment [54].

During the entire data collection period of more than 2 years, all 18 crystals successfully measured the heat signals. The energy resolution of all crystals ranged from 10 to 20 keV FWHM, with no degradation in the energy resolution observed for the whole period. However, one detector's light sensor malfunctioned, and it was excluded from the background spectrum analysis.

3.3 AMoRE-II

The primary experiment of AMoRE, AMoRE-II, is currently in preparation at Yemilab, with data collection scheduled to commence in 2024. Due to the extended time required to grow enriched crystals with limited amount of enriched powder, AMoRE-II will be conducted in two stages. The initial stage will utilize 90 LMO crystals (27 kg) for approximately 1 year, followed by a subsequent stage employing 360 LMO crystals (157 kg). We will verify the energy resolution and background levels by comparing simulation results with

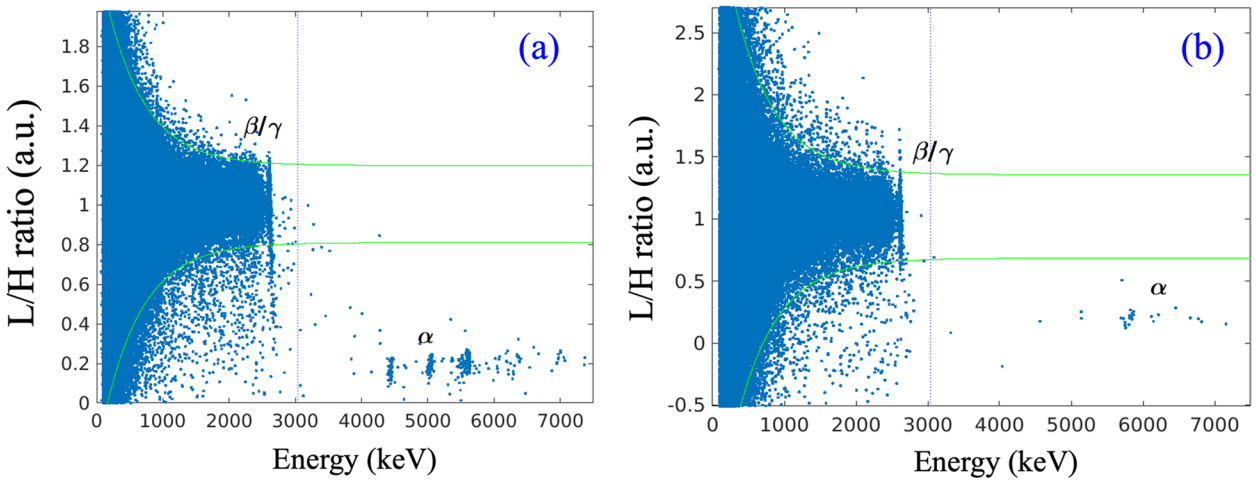

Fig. 4 **a** Light/heat ratio versus energy for a CMO crystal detector. **b** Same figure for an LMO crystal detector [52]. The vertical solid line is the energy of $0\nu\beta\beta$. The ROI is ±1.5 FWHM of the energy and the backgrounds near ROI are mainly from radioimpurity, neutron capture, and surface alpha leakage to the beta band

data from the first stage and work to improve detector performance. Two different sizes of cylindrical LMO crystals will be used for AMoRE-II: one measuring 5 cm and the other measuring 6 cm in both diameter and height.

Utilizing larger-size crystals and reducing the number of channels provides advantages. One concern was the so-called pile-up phenomenon, where the random coincidence event rate due to two neutrino double beta decay increases as the crystal volume expands. Another concern was the potential increase in non-uniform response as the crystal volume grows, which could adversely affect energy resolution and $\beta\alpha$ discrimination. We compared the performance of LMO crystals of different sizes and surface treatments, finding that crystals with a diffusive surface exhibited minimal size-related effects, resulting in significantly reduced non-uniform response regardless of their sizes.

The energy resolution for both crystal sizes was found to be similar, approximately 8 keV full-width-half-maximum (FWHM) for the 2.614 MeV γ-ray peak in the best cases, and better than 15 keV FWHM in all cases within the temperature range of 10 to 30 mK as shown in Fig. 5. Furthermore, the β and α discrimination of the 6 cm crystal detector was as effective as the smaller one, with a discrimination power, defined as the difference of β/α peak positions divided by the quadratic sum of their Gaussian widths, exceeding 10 at around 5 MeV, as illustrated in Fig. 5. Studies also indicated that the expected pile-up event rate for the 6 cm crystal is below 3×10^{-5} ckky, using multivariate analysis techniques such as boosted decision trees [55].

By February 2024, approximately 100 kg of crystals (270 crystals) have been produced at the Center for Underground Physics (CUP/IBS) [56] and the Nikolaev Institute of Inorganic Chemistry (NIIC). All crystals required for the second stage of AMoRE-II are expected to be ready by mid-2025. Raw materials for crystal growth, including MoO_3 and Li_2CO_3 powder, have undergone purification at CUP/IBS to reduce radioactivity [57–59].

To accommodate hundreds of crystal detector modules, a new pulse tube dilution refrigerator was manufactured and delivered by Leiden Cryogenics. The innermost volume of the cryogenic system measures approximately 1 m in both diameter and height, capable of containing 76 towers of 12 crystal detector modules each, with the current module design. The cryogenic system is designed to support up to 3.3 tons of lead, copper, and crystals in the inner vacuum chamber, with thousands of cables passing through the cooling stages. To efficiently cool such a large volume and mass, the refrigerator is equipped with 3 pulse tubes, and the cooling stages make soft contact with each other using copper foils. Dampers, including spring-suspended and Eddy current dampers in the cryostat, and air dampers at the supporting structure, are employed to reduce vibration resulting from pulse tube operation [60]. The system has undergone ground laboratory testing, achieving a temperature of 6 mK without wiring, and is scheduled for relocation to Yemilab in May 2024.

Inside the inner vacuum chamber, a 26-cm-thick lead shielding is placed over the crystal detector towers. The external shielding structure is currently under construction at Yemilab. The sides and bottom of the refrigerator are enveloped in a shielding layer sequence, beginning with an innermost layer of 1 cm boric acid rubber, followed by 25 cm of lead, another 1 cm of boric acid rubber, and a substantial 70 cm of polyethylene, as depicted in Fig. 6. The outermost layer consists of muon counter panels constructed from plastic scintillator. Preliminary measurements using the bottom panels indicate a muon rate of approximately 1 muon/cm^2/s, which is about one fourth of the rate at Y2L [31, 61]. Above the cryo-chamber, the space is dedicated to the detector control room and the data acquisition

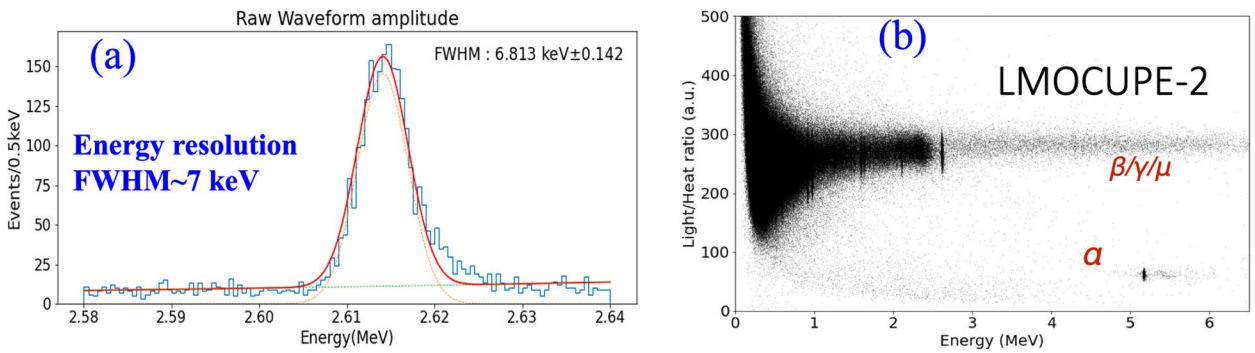

Fig. 5 **a** Energy spectrum of the heat channel for a 6 cm crystal detector in response to a 2.614 MeV gamma signal. **b** Light/heat ratio versus energy for a 5 cm LMO crystal detector. The beta/gamma band is distinctly separated from the alpha band by more than 10 standard deviations (σ)

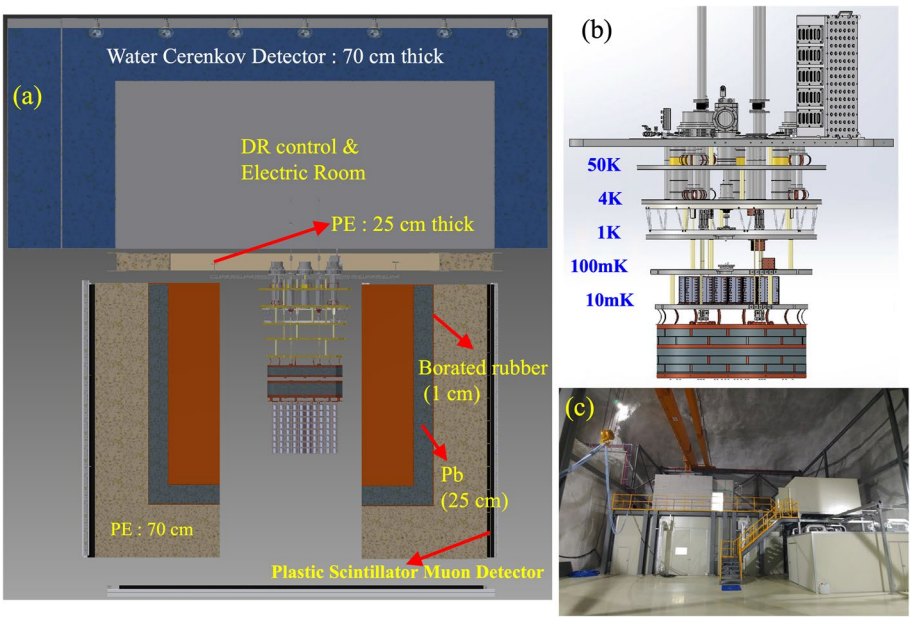

Fig. 6 **a** Schematics of the shielding structure of the AMoRE-II experiment. **b** Layout of the cryostat and dilution refrigerator used in AMoRE-II. **c** Photograph of the AMoRE hall at Yemilab

system, encased within a 70–80-cm-thick water tank that serves as passive shielding and houses the Cherenkov muon detector. Radon-free air is circulated into the vinyl housing that surrounds the cryo-chamber.

Materials and components for detector modules and shielding were carefully chosen and measured for their radioactivity levels [62]. The expected background around $Q_{\beta\beta}$ is estimated to be less than 2×10^{-4} ckky, based on an extensive detector simulation using radioassay results [63]. Several active items have been identified, and further reduction in background levels are possible to meet the target of 2×10^{-4}. This level corresponds to less than one background event after 500 kg.year of crystal mass-time exposure, assuming a 10 keV FWHM energy resolution. The fine energy resolution becomes increasingly important due to the β-decay of ^{214}Bi emitting a 3050-keV γ-ray, with expected background level higher than 10^{-3} ckky. The primary contributors to this background are ^{238}U elements in lead and the radon in the air. Efforts are underway to procure the most radio-pure lead and minimize airborne radon levels.

Another important concern regarding background is surface contamination of crystals and copper holders, which is chanllenging to estimate via radioassay or simulations. Steps are being taken to maintain cleanliness throughout the material handling processes, including crystal production, surface treatment, detector module assembly, storage, and transportation.

The first stage of AMoRE-II is scheduled to run for approximately 1 year, with an additional year allocated for upgrading to the next phase, followed by the second stage running for more than 5 years. After approximately 7 years of AMoRE-II data collection, an exposure equivalent to about 500 kg.year of ^{100}Mo mass-time exposure, roughly corresponding to 3×10^{27} of ^{100}Mo-atom.year, is expected. With the anticipated background of 10^{-4} ckky and 10 keV FWHM energy resolution, the observation of a $0\nu\beta\beta$ peak signal for a half-life of 5×10^{26} years is expected at a 3-σ confidence level as shown in Fig. 7 [63, 64]. This half-life sensitivity corresponds to the effective Majorana mass upper limit of 18–31 meV according to the prediction using Eq. 1 [65].

4 COSINE——a dark matter direct detection experiment

Since its first indications of an annual modulation signal in 1998 [66], the DAMA/LIBRA collaboration has consistently reported a positive signature from their annual modulation analysis for over 25 years [67–70], using a low-background NaI(Tl) detector array that can be interpreted as interactions between weekly interacting massive particles (WIMPs) and nuclei [71, 72]. However, no other experiment has detected any evidence of dark matter interaction, despite employing more advanced technologies and achieving lower cross-sectional limits for canonical WIMP dark matter models [3]. Therefore, it is imperative to obtain an unambiguous verification of the

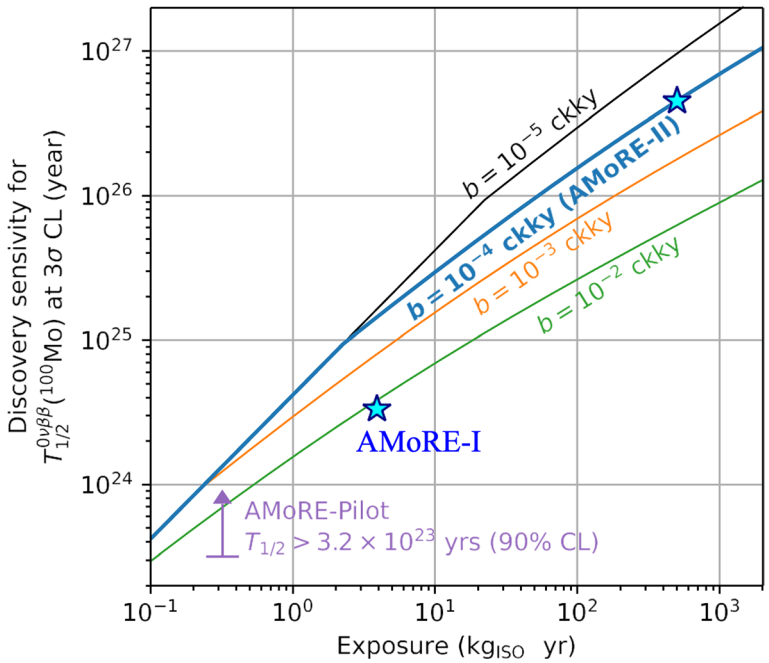

Fig. 7 The discovery sensitivity at the 90% confidence level as a function of exposure in unit of $kg_{isotope}$ · year. AMoRE-I had about 3.9 $kg_{isotope}$ · year and AMoRE-II will have 500 $kg_{isotope}$ · year with an expected background level of 10^{-4} ckky

DAMA/LIBRA signal through an independent experiment using same NaI(Tl) crystals.

Experimental efforts by several groups using NaI(Tl) as the target medium are currently underway [73–78], with two operational experiments, COSINE-100 [75] and ANAIS-112 [79]. Although these experiments have produced interesting physics results [27, 80–84], the background levels they have achieved are higher than those of DAMA/LIBRA [85–87]. This high background is a significant obstacle to drawing unambiguous conclusions. While several efforts have demonstrated the feasibility of producing low-background NaI(Tl) crystals that reach the background levels of DAMA/LIBRA [88–91], the mass production of large-sized crystals with similarly low background levels has not yet been achieved.

Fig. 8 Photo of NaI(Tl) crystals used for the COSINE-100 experiment

4.1 COSINE-100 experiment

The COSINE-100 experiment [75] aims to reproduce the DAMA/LIBRA's annual modulation signals using the same NaI(Tl) crystals. This experiment began physics operation in October 2016 with an array of 106 kg low-background NaI(Tl) crystal detectors, as shown in Fig. 8, located at 700 m deep Yangyang underground laboratory [31]. The first physics analysis, based on initial 59.5 days of data, extracted dark matter interactions from low-energy event rate spectra, building upon a solid understanding of detector's backgrounds [85, 87]. The analysis showed inconsistent results with DAMA/LIBRA when attempting to explain the DAMA/LIBRA's signal using a spin-independent interaction between WIMPs and sodium or iodine nuclei within the framework of the standard halo model [27]. These findings have been further reinforced by 1.7 years of COSINE-100 data, which do not favor various dark matter interpretations of DAMA/LIBRA's observations [82].

Model-independent searches for an annual modulation signal using 1.7 years of data [80], as well as a 3-years updated analysis [81], have been reported. However, these searches were still not sensitive enough to

conclusively challenge the DAMA/LIBRA's observation. One interesting approach, adopting a similar analysis technique to DAMA/LIBRA, was applied to the COSINE-100 data, revealing a significant annual modulation signal [92]. However, this signal was attributed to an incorrect model of the time-dependent background, specifically a simple 1-year average, but with an opposite modulation phase [92]. Simulated experiments for DAMA/LIBRA's data, assuming the same background composition as COSINE-100, surprisingly induced a consistent annual modulation amplitude, although the modulation phase was exactly opposite.

In addition to typical WIMP dark matter searches for elastic scattering, COSINE-100 performed extended searches for dark sector particles. The search for WIMP-^{127}I inelastic scattering, which produces a 57.6-keV γ-ray accompanying the nuclear recoil, in the energy range of 35 keV–85 keV, did not yield any signals from 1.7 years of COSINE-100 data, resulting in world-best limits on the WIMP-proton spin-dependent interaction via inelastic scattering [93]. In the energy range of 10 keV–1000 keV, a search for excess signals due to bosonic super-WIMPs has been conducted with null results [94]. In this search, we included the Compton-like process [95] for the first time in the world, leading to comparative limits for mass greater than 200 keV, compared to the current best results from the GERDA experiment [96]. Further searches for higher energy signals caused by boosted dark matter have been conducted for both inelastic [97] and elastic [98] interactions, with null observations in the signal regions above 4 MeV. An annual modulation study due to the distance between the Sun and Earth was performed to search for solar bosonic dark matter [99].

4.2 COSINE-100U (upgrade) at Yemilab

The COSINE-100 experiment concluded in March 2023 for relocation of the experimental site to Yemilab [30] as well as upgrading the NaI(Tl) detector assembly for enhanced light output [100]. Decommissioning of the detector was completed by October 2023, as shown in Fig. 9. All materials were delivered to Yemilab. We prepared a warehouse-type refrigerator for the operation of upgraded COSINE-100, called COSINE-100U experiment, as depicted in Fig. 9e, taking advantages of increased light output and improved pulse shape discrimination of nuclear recoil event [101]. Installation of shielding structure began in January 2024, as shown in Fig. 9f and g. With upgraded NaI(Tl) crystal detectors, we plan to commence physics operation of the COSINE-100U by September 2024.

We have developed a novel crystal encapsulation technique that improves light collection efficiency with a

Fig. 9 Photos taken during the decommissioning of the COSINE-100 detector at the Yangyang underground laboratory are presented in **a**–**d**. **e** The COSINE-100U detector room at Yemilab for operation at −30°C. Photos of shield installation for COSINE-100U at Yemilab inside the detector room are shown in **f** and **g**

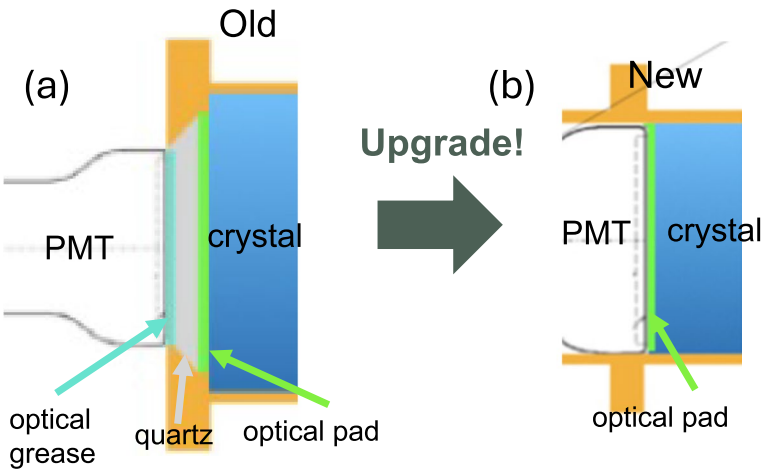

Fig. 10 **a** Light coupling between NaI(Tl) crystals and PMTs utilized in the COSINE-100 experiment. **b** Enhanced light coupling method without quartz windows implemented for the NEON experiment

simplified design by attaching the PMTs directly to the crystal [100], as schematically shown in Fig. 10. In the case of the NEON experiment, we use 3-inch diameter crystals directly coupled to 3-inch PMTs, achieving approximately 22 number of photoelectrons (NPE) per unit keV (NPE/keV) was achieved [102], while the COSINE-100 crystals had approximately 15 NPE/keV [75]. In the COSINE-100U experiment, we aim to improve the light collection efficiency with a similar concept. However, the diameters of the crystals, which range from 4.2 inches to 5 inches, are much larger than PMT diameter. We then machine the crystal edges to match with 3-inch diameter PMTs, as depicted in Fig. 11. The observed light yield of the COSINE-100 crystal-1 was 14.9 ± 1.5 NPE/keV [75], but the improved encapsulation design applied to this crystal obtained 21.6 ± 0.6 NPE/keV, approximately 45 % increase in light yield. We expect that the energy threshold can be lowered, and sensitivity for low-mass dark matter particle searches significantly improved. By March 1, 2024, four of the

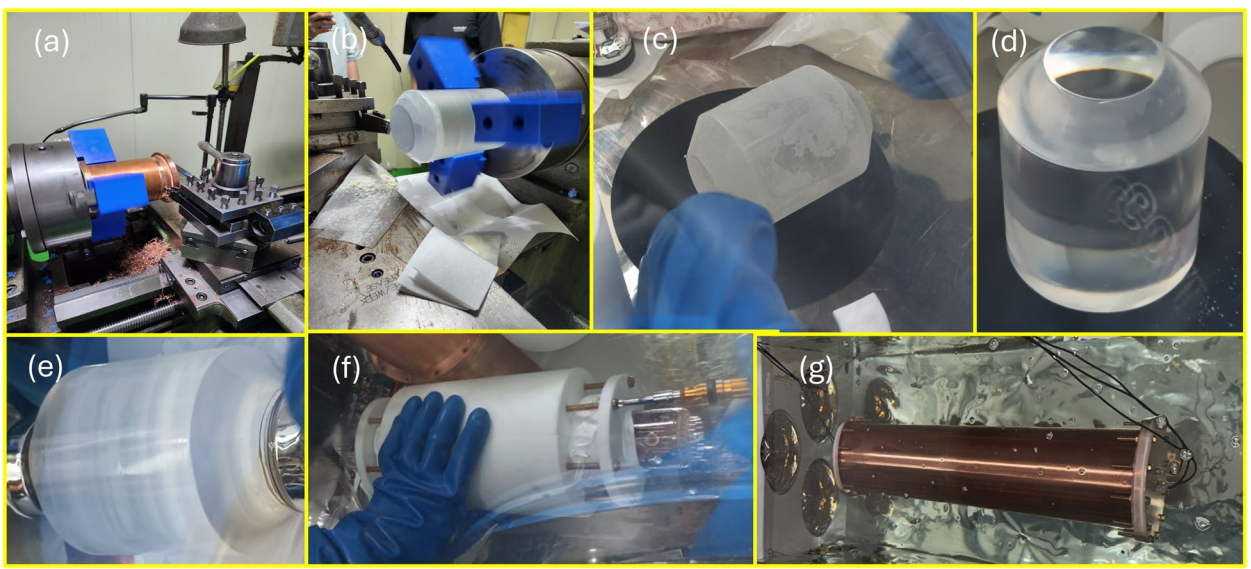

Fig. 11 An example of COSINE-100U crystal encapsulation was performed for crystal-1. **a** Removal of the copper case of the crystal using a lathe machine. **b** Machining of two edges of the 5-inch-diameter crystal to collimate with 3-inch PMTs at a 45° angle using the lathe machine. **c** Delivery of the machined crystal to a low-humidity glove box. **d** Polishing of the crystal. **e** Attachment of the crystal to 3-inch PMTs. **f** Mechanical assembly of the crystal and PMTs with PTFE structures. **g** Application of a copper case to prevent humidity or liquid scintillator from leaking into the crystal

eight COSINE-100 crystals were assembled using a similar technique. We plan to upgrade all crystals by April 30, 2024, for starting physics operation of the COSINE-100U at Yemilab in May 2024.

4.3 COSINE-200 experiment

Although interesting checks on DAMA/LIBRA's observation have been reported using COSINE-100 data, an unambiguous conclusion regarding DAMA/LIBRA's findings has not yet been reached due to the background levels of the crystals [87], which are 2–3 times higher than those of DAMA/LIBRA. As part of an effort to upgrade the ongoing COSINE-100 and COSINE-100U experiments to the next-phase COSINE-200 experiment [103], we have developed in-house technologies for low-background NaI(Tl) crystal growth. Initial chemical purification of raw NaI powder, using a recrystallization method, has resulted in a significant reduction of K and Pb impurities [104]. A large-scale facility for this process has already been assembled [105] and is in stable operation [106]. We have demonstrated the ability to achieve sufficiently low levels of ^{40}K and ^{210}Pb through proof-of-concept crystallization using a small crystal grower, producing approximately 1 kg-size crystal ingots that we match or exceed the low background levels of DAMA/LIBRA [89, 91]. We are currently developing crystallization for a 10 kg-size detector.

Based on the improved light collection in the COSINE-100U detectors and proof of a low-background crystallization technique, the next phase COSINE-200 experiment will verify DAMA/LIBRA's signal without any ambiguity. In addition to testing DAMA/LIBRA's signal, high light yield detector technology will provide world-competitive sensitivity for low-mass dark matter, especially for the spin-dependent WIMP-proton interaction, as depicted in Fig. 12. This could open up a new window of tonne-scale solid detectors using NaI(Tl) crystals, which are unique target materials for direct dark matter search experiments.

5 Future large neutrino detector

The construction of Yemilab includes the excavation of a large cylindrical cavern of 20 m in diameter and 20 m in height, intended to accommodate a potential future large neutrino detector based on liquid scintillator counter [30]. A conceptual design aims to fill this cavern with approximately 2.2 kton of target liquid scintillator counter (LSC). Such a detector would be capable of studying various physics topics, including astrophysical neutrino studies, neutrino property measurements, and searches for particles in dark sector.

5.1 Conceptual design of the large neutrino detector

Because we excavated the cavern in the cylindrical shape, it is natural to design a cylindrical detector for efficient use of space. This detector can be composed of three distinct areas: main target, buffer, and veto, from inner to outer, as shown in Fig. 13. The target area consists of a 15-m height and 15-m-diameter cylindrical space that installs 2.2 kton liquid scintillator. Liquid scintillator is the most widely used target for neutrino measurements in the 1–10 MeV energy range [108]. In Korea, RENO [16] and NEOS [109] experiments have used LAB-based liquid scintillator to study neutrino oscillation from nuclear reactors, providing us with considerable expertise. The buffer area consists of 1.1 kton of mineral oil covered by a few thousands 50 cm diameter PMTs. The veto area is filled with 2.4 kton of pure water with PMTs that will act as muon veto detector, observing Cherenkov radiation of the energetic muons.

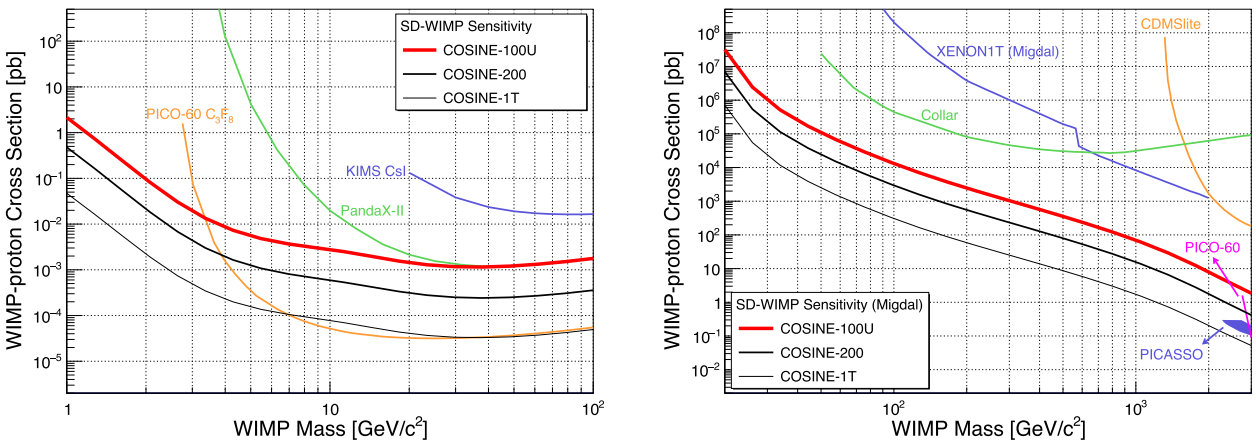

Fig. 12 Sensitivities of future COSINE experiments on WIMP-proton spin-dependent interaction without Migdal effect (left) and with Migdal effect (right) [107]

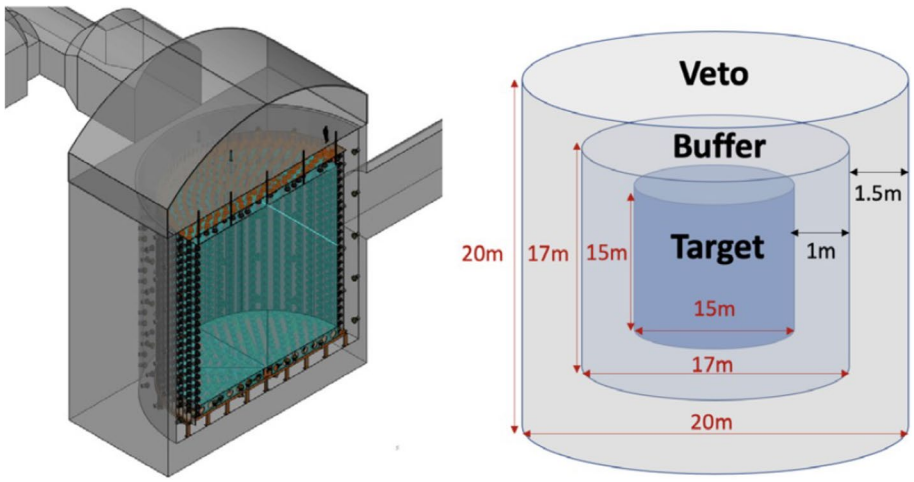

Fig. 13 A conceptual design of the large neutrino detector consisting of three layers of cylindrical regions. The innermost "Target" region would be filled with 2.2 kton liquid scintillator, and it is surrounded by "Buffer" region filled with 1.1 kton mineral oil, where PMTs will be attached to the stainless steel vessel walls. The outermost "Veto" region will be filled with 2.4 kton pure water to veto cosmic muons

Various topics related to neutrinos can be studied. As a neutrino telescope, precision measurements of solar neutrino, detecting neutrinos from supernova burst, and observing geoneutrino can be investigated. By adopting an electron accelerator, searches for dark photon and axion-like particles would be beneficial [110]. With a strong neutrino source such as IsoDAR [111] or a high-activity β-decay source [112] near the large neutrino detector, one can explore sterile neutrino parameter spaces suggested by various anomalies from neutrino oscillation experiments. It is also possible to extend physics program to include the study of neutrinoless double beta decay by loading double beta decay elements into the liquid scintillator, similar as SNO+ experiment [113].

5.2 Solar neutrinos

Solar neutrinos are produced in the core of the Sun by nuclear reactions, wherein hydrogen is transformed into helium and heavier elements. The dominant sequence producing solar neutrinos is the proton-proton chain, while the carbon-nitrogen-oxygen (CNO) cycle also emits neutrinos [114]. Solar neutrinos produced from the atomic elements are named *pp*, ^{7}Be, *pep*, ^{8}B, and CNO neutrinos. Solar neutrinos have been extensive studied by experiments such as Borexino, Super-Kamiokande, and SNO. Among these, the Borexino experiment has observed the most solar neutrinos, excluding *hep* neutrino, and achieved the most precise measurements for solar neutrinos [115].

The success of the Borexino experiment in measuring nearly all types of solar neutrinos can be attributed to two primary reasons: firstly, the use of a liquid scintillator as the target medium for solar neutrinos within MeV scale low-energy spectrum, and secondly, through extensive research and development efforts to purify the liquid scintillator to extremely high levels of purity, enabling measurements down to energies below 1 MeV. Borexino, equipped with a 300-ton liquid scintillator detector, conducted solar neutrino data collection from 2007 to 2021, excluding 4 years dedicated to upgrade periods occurring on two separate occasions. However, due to the relatively compact size of the detector, statistical uncertainties dominate, limiting the precision of the solar neutrino measurements.

In contrast, the large neutrino detector at Yemilab boasts a volume approximately eight times larger than that of the Borexino detector. With similar time scale measurements, the eight times larger dataset can reduce the statistical uncertainties by approximately a factor of 3. High-precision measurements of solar neutrinos will allow us to test the standard solar model and explore new physics possibilities.

5.3 Dark photon search

The dark photon is a well motivated hypothetical dark sector particle that connects the dark sector to the visible universe. The pioneering search for dark photon was performed by E137 beam dump experiment [116, 117]. This particle has garnered increased interest with extensive investigations from fixed-target accelerator experiments, $e^{+}e^{-}$ colliders, reactors, and astrophysical measurements [118, 119].

The large neutrino detector at Yemilab has great potential to search for dark photon in the MeV-scale mass range by adopting a 100 MeV electron accelerator [110]. Figure 14 illustrates a schematic diagram where 100 MeV electrons, accelerated by an electron

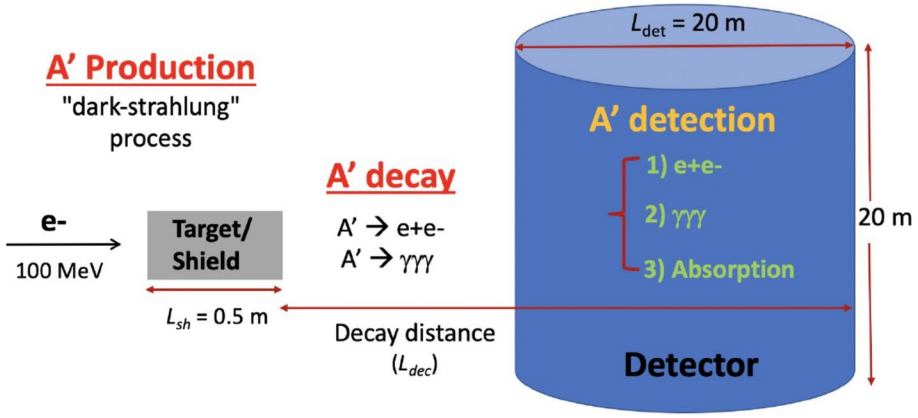

Fig. 14 Schematics of experimental setup for dark photon search. The 100 MeV electron beam (100 kW) from a linac strikes 50-cm-thick tungsten target, and dark photons could be produced via a dark-strahlung process. The produced dark photons can be detected in visible decay channels or a Compton-like scattering. This figure is from Ref. [110]

linac, strike a tungsten target. When an electron beam strikes a target with an atomic number Z, dark photons (A) can be produced through the so called dark-strahlung process: $e^- + Z \rightarrow e^- + Z + A$ [120].

If dark photon mass (m_A) is greater than two times of electron mass ($2m_e$), dark photons could decay into the visible e^+e^- final state. If $m_A < 2m_e$, the only visible decay mode is the $\gamma\gamma\gamma$ channel. Direct scattering of the dark photon and electron can produce γ through a Compton-like scattering process ($e^- + A \rightarrow e^- + \gamma$). We can observe all three of these channels with the large neutrino detector. We evaluate detection sensitivities of the dark photon assuming 1 year of data with 100 MeV linar accelerator with a beam current of 100 kW. For the dark photon mass below 100 MeV, the Yemilab experiment can provide the world's best sensitivity [110].

5.4 Sterile neutrino search

Neutrinos have a unique opportunity to communicate with fermions outside the Standard Model through mass mixing, such as singlet fermions refer to as sterile neutrino. The possibility of the existence of sterile neutrinos has been suggested by several neutrino oscillation anomalies, beginning with the LSND and MiniBooNE experiments from accelerator-based neutrino beams as well as experiments using nuclear reactors and intense samples of radioactive isotopes [121].

IsoDAR@Yemilab is a proposed experiment aimed at resolving neutrino oscillation anomalies and searching for physics beyond Standard Model [122, 123]. This can be achieved by producing neutrinos from the β-decay of ^{8}Li, produced by bombarding a ^{9}Be target with 60 MeV protons accelerated by a cyclotron. In this process, direct production of ^{8}Li is possible, but a significantly larger number of neutrons are produced. By surrounding ^{9}Be target with ^{7}Li Sleeve, neutrons can be captured to produce even more ^{8}Li, as illustrated in Fig. 15. This IsoDAR source is located approximately 17 m far from the large neutrino detector at Yemilab. Geant4-based simulation studies indicate that we can expect 2 million inverse β

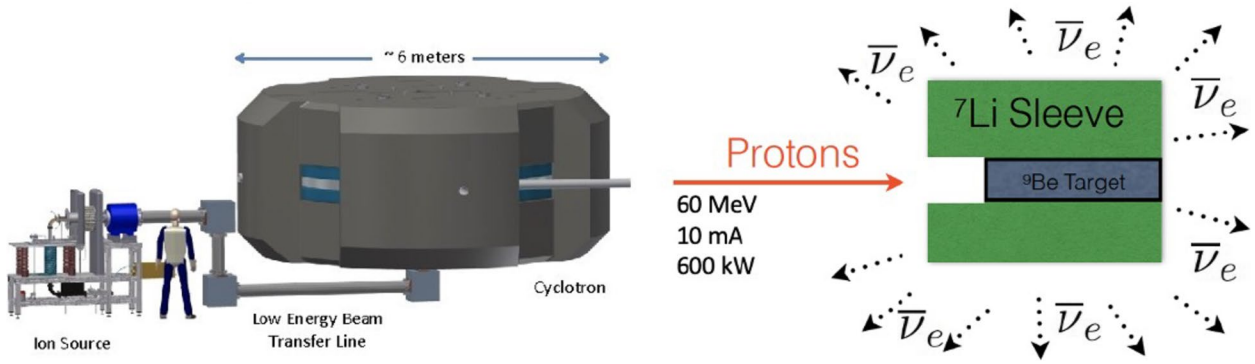

Fig. 15 Schematics of IsoDAR neutrino source set up. The 60 MeV proton beam (10 mA, 600 MW) produced by a cyclotron strikes ^{9}Be target that generate large flux neutrons. The neutrons are captured by ^{7}Li Sleeve and produce ^{8}Li. Electron antineutrions are produced by β-decay of ^{8}Li

decay signals over 5 years of operation, assuming 60 MeV protons with a beam power of 600 kW. With short-base line (17 m) oscillation study, IsoDAR@Yemilab experiment can explore all parameter spaces allowed by neutrino oscillation anomalies [124].

In addition to the search for the sterile neutrinos, the IsoDAR@Yemilab experiment can explore the existence of a new bosonic state, the lighter mediator of mass 16.7 MeV, as claimed in Ref. [125]. It can also investigate the 5 MeV bump observed in reactor neutrinos and measure elastic scattering of $\bar{\nu_e} - e^-$, providing insights into electroweak mixing angle at low energy regimes, as detailed in Ref. [124].

Alternatively, instead of using IsoDAR neutrino source with a high-intensity proton cyclotron, one can consider a high-activity β source similar to the SOX experiment, using the Borexino detector [112]. We propose using a 100 kCi ^{144}Ce source positioned 4 m away from the large neutrino detector. Although the expected sensitivity to search for sterile neutrino is much lower than that of the IsoDAR neutrino source, this experiment can still explore many of the neutrino anomalies within the sterile neutrino parameter space.

6 Conclusion

In Korea, we have initiated non-accelerator astroparticle physics research with the construction of Y2L and the KIMS dark matter search experiment since 2003. This endeavor was significantly advanced with the completion of the dedicated underground research laboratory, Yemilab, in 2022. Although Yemilab is not as deep as other leading underground laboratories such as CJPL, LNGS, and SNOlab, it is positioned to conduct competitive experiments in areas such as neutrinoless double beta decay, low mass dark matter searches, and sterile neutrino searches, thereby holding its ground against other top leading experiments. The AMoRE and COSINE projects are set to further the pursuit of new parameter searches, potentially shedding light on unresolved questions beyond the Standard Model. Looking ahead, our long-term plan is to engage in next-generation experiments focusing on neutrinoless double beta decay and dark matter searches, in addition to continuing our efforts in sterile neutrino searches.

Acknowledgements
We thank the Korea Hydro and Nuclear Power (KHNP) Company for providing underground laboratory space at Yangyang. We acknowledge the outstanding contributions and publications of all the collaborators from the AMoRE, COSINE-100, and IsoDAR@Yemilab projects. Our sincere thanks go to all members of the Yemilab construction team for their dedication and hard work in completing the construction of Yemilab.

Authors' contributions
YK and HSL wrote the manuscript. All authors proofread and approved the final version of the manuscript.

Funding
This work was supported by the Institute for Basic Science (IBS) under project code IBS-R016-D1 and IBS-R016-A1.

Availability of data and materials
The data and figures from published materials belongs to the authors of each publication. The other data and figures are available from the authors upon reasonable request.

Declarations

Competing interests
The authors declares that they have no competing interests.

Received: 1 April 2024 Accepted: 31 August 2024
Published online: 16 September 2024

References

1. G. Aad et al., Observation of a new particle in the search for the Standard Model Higgs boson with the ATLAS detector at the LHC. Phys. Lett. B **716**, 1–29 (2012). https://doi.org/10.1016/j.physletb.2012.08.020. arXiv:1207.7214
2. S. Chatrchyan et al., Observation of a new boson at a mass of 125 GeV with the CMS experiment at the LHC. Phys. Lett. B **716**, 30–61 (2012). https://doi.org/10.1016/j.physletb.2012.08.021. arXiv:1207.7235
3. R.L. Workman et al., Review of particle physics. PTEP **2022**, 083–01 (2022). https://doi.org/10.1093/ptep/ptac097
4. R.N. Mohapatra et al., Theory of neutrinos: A white paper. Rept. Prog. Phys. **70**, 1757–1867 (2007). https://doi.org/10.1088/0034-4885/70/11/R02. arXiv:hep-ph/0510213
5. N. Aghanim et al., Planck 2018 results. VI. Cosmological parameters. Astron. Astrophys. **641**, 6 (2020). https://doi.org/10.1051/0004-6361/201833910. arXiv:1807.06209
6. D. Clowe et al., A direct empirical proof of the existence of dark matter. Astrophys. J. **648**, 109 (2006). https://doi.org/10.1086/508162
7. A.G. Riess et al., Observational evidence from supernovae for an accelerating universe and a cosmological constant. Astron. J. **116**, 1009–1038 (1998). https://doi.org/10.1086/300499. arXiv:astro-ph/9805201
8. A. Arbey, F. Mahmoudi, Dark matter and the early Universe: A review. Prog. Part. Nucl. Phys. **119**, 103865 (2021). https://doi.org/10.1016/j.ppnp.2021.103865. arXiv:2104.11488
9. G. Bertone, D. Hooper, J. Silk, Particle dark matter: Evidence, candidates and constraints. Phys. Rept. **405**, 279–390 (2005). https://doi.org/10.1016/j.physrep.2004.08.031. arXiv:hep-ph/0404175
10. M. Schumann, Direct detection of WIMP dark matter: Concepts and status. J. Phys. G **46**(10), 103003 (2019). https://doi.org/10.1088/1361-6471/ab2ea5. arXiv:1903.03026
11. Y.K. Semertzidis, S. Youn, Axion dark matter: How to see it? Sci. Adv. **8**(8), 9928 (2022). https://doi.org/10.1126/sciadv.abm9928. arXiv:2104.14831
12. Q.R. Ahmad et al., Measurement of the rate of $\nu_e + d \rightarrow p + p + e^-$ interactions produced by ^{8}B solar neutrinos at the Sudbury Neutrino Observatory. Phys. Rev. Lett. **87**, 071301 (2001). https://doi.org/10.1103/PhysRevLett.87.071301. arXiv:nucl-ex/0106015
13. Y. Fukuda, et al., Evidence for oscillation of atmospheric neutrinos. Phys. Rev. Lett. **81**, 1562–1567 (1998). https://doi.org/10.1103/PhysRevLett.81.1562. arXiv:hep-ex/9807003
14. S. Abe et al., Precision measurement of neutrino oscillation parameters with KamLAND. Phys. Rev. Lett. **100**, 221803 (2008). https://doi.org/10.1103/PhysRevLett.100.221803. arXiv:0801.4589
15. K. Abe et al., Indication of electron neutrino appearance from an accelerator-produced off-axis muon neutrino beam. Phys. Rev. Lett. **107**, 041801 (2011). https://doi.org/10.1103/PhysRevLett.107.041801. arXiv:1106.2822
16. J.K. Ahn et al., Observation of reactor electron antineutrino disappearance in the RENO experiment. Phys. Rev. Lett. **108**, 191802 (2012). https://doi.org/10.1103/PhysRevLett.108.191802. arXiv:1204.0626

17. R.N. Mohapatra, G. Senjanovic, Neutrino mass and spontaneous parity nonconservation. Phys. Rev. Lett. **44**, 912 (1980). https://doi.org/10.1103/PhysRevLett.44.912
18. J. Schechter, J.W.F. Valle, Neutrino masses in SU(2) x U(1) theories. Phys. Rev. D **22**, 2227 (1980). https://doi.org/10.1103/PhysRevD.22.2227
19. A.A. Aziz et al., Progress in nuclear astrophysics of east and southeast Asia. AAPPS Bull. **31**(1), 18 (2021). https://doi.org/10.1007/s43673-021-00018-z. arXiv:2108.03814
20. X. Zhou, J. Yang, Status of the high-intensity heavy-ion accelerator facility in China. AAPPS Bull. **32**(1), 35 (2022). https://doi.org/10.1007/s43673-022-00064-1
21. B. Hong, Status of the RAON project in Korea. AAPPS Bull. **33**(1), 3 (2023). https://doi.org/10.1007/s43673-022-00074-z
22. A. Tamii, N. Kobayashi, Studies on electromagnetic dipole responses of atomic nuclei at RCNP. AAPPS Bull. **34**(1), 7 (2024). https://doi.org/10.1007/s43673-023-00108-0
23. L. Baudis, J. Hall, K.T. Lesko, J.L. Orrell, Snowmass 2021 Underground Facilities and Infrastructure Overview Topical Report (2022). arXiv:2212.07037
24. Y. Kim, Deep underground laboratories - Multidisciplinary research. PoS **TAUP2023**, 298 (2024). https://doi.org/10.22323/1.441.0298
25. H.S. Lee, Dark matter search with CsI(Tl) crystals. PhD thesis, Seoul Natl. U. (2007). https://inspirehep.net/files/c4ea3ecd1a20a5cddac93b2b497ea55d
26. S.C. Kim et al., Low energy fast events from radon progenies at the surface of a CsI(Tl) scintillator. Astropart. Phys. **35**, 781–784 (2012). https://doi.org/10.1016/j.astropartphys.2012.03.005
27. G. Adhikari et al., An experiment to search for dark-matter interactions using sodium iodide detectors. Nature **564**(7734), 83–86 (2018). https://doi.org/10.1038/s41586-018-0739-1
28. V. Alenkov et al., First results from the AMoRE-Pilot neutrinoless double beta decay experiment. Eur. Phys. J. **C79**(9), 791 (2019). https://doi.org/10.1140/epjc/s10052-019-7279-1. arXiv:1903.09483
29. A. Agrawal et al., Improved limit on neutrinoless double beta decay of \ mohundred~ from AMoRE-I (2024). arXiv:2407.05618
30. K.S. Park, Y.D. Kim, K.M. Bang, H.K. Park, M.H. Lee, J. So, S.H. Kim, J.H. Jang, J.H. Kim, S.B. Kim, Construction of yemilab. Front. in Phys. **12**, 1323991 (2024). https://doi.org/10.3389/fphy.2024.1323991. arXiv:2402.13708
31. H. Prihtiadi et al., Muon detector for the COSINE-100 experiment. JINST **13**(02), 02007 (2018). https://doi.org/10.1088/1748-0221/13/02/T02007
32. H.W. Bae, E.J. Jeon, Y.D. Kim, S.W. Lee, Neutron and muon-induced background studies for the AMoRE double-beta decay experiment. Astropart. Phys. **114**, 60–67 (2020). https://doi.org/10.1016/j.astropartphys.2019.06.006. arXiv:1812.07476
33. Q.R. Ahmad et al., Direct evidence for neutrino flavor transformation from neutral current interactions in the Sudbury Neutrino Observatory. Phys. Rev. Lett. **89**, 011301 (2002). https://doi.org/10.1103/PhysRevLett.89.011301. arXiv:nucl-ex/0204008
34. M. Aker et al., Direct neutrino-mass measurement with sub-electronvolt sensitivity. Nature Phys. **18**(2), 160–166 (2022). https://doi.org/10.1038/s41567-021-01463-1. arXiv:2105.08533
35. E. Majorana, Teoria simmetrica dell'elettrone e del positrone. Nuovo Cim. **14**, 171–184 (1937). https://doi.org/10.1007/BF02961314
36. W.H. Furry, On transition probabilities in double beta-disintegration. Phys. Rev. **56**, 1184–1193 (1939). https://doi.org/10.1103/PhysRev.56.1184
37. J. Schechter, J.W.F. Valle, Neutrinoless double beta decay in SU(2) x U(1) Theories. Phys. Rev. D **25**, 2951 (1982). https://doi.org/10.1103/PhysRevD.25.2951
38. M. Fukugita, T. Yanagida, Baryogenesis without grand unification. Phys. Lett. **B174**, 45–47 (1986). https://doi.org/10.1016/0370-2693(86)91126-3
39. F.F. Deppisch, L. Graf, J. Harz, W.-C. Huang, Neutrinoless double beta decay and the baryon asymmetry of the universe. Phys. Rev. D **98**, 055029 (2018). https://doi.org/10.1103/PhysRevD.98.055029
40. C. Giunti, C.W. Kim, Fundamentals of neutrino physics and astrophysics (Univ. Pr., Oxford, 2007), p. 710
41. M. Doi, T. Kotani, E. Takasugi, Double beta decay and Majorana neutrino. Prog. Theor. Phys. Suppl. **83**, 1 (1985). https://doi.org/10.1143/PTPS.83.1
42. I. Esteban, M.C. Gonzalez-Garcia, M. Maltoni, T. Schwetz, A. Zhou, The fate of hints: Updated global analysis of three-flavor neutrino oscillations. JHEP **09**, 178 (2020). https://doi.org/10.1007/JHEP09(2020)178. arXiv:2007.14792
43. M.A. Acero et al., Improved measurement of neutrino oscillation parameters by the NOvA experiment. Phys. Rev. D **106**(3), 032004 (2022). https://doi.org/10.1103/PhysRevD.106.032004. arXiv:2108.08219
44. F. An et al., Neutrino physics with JUNO. J. Phys. **G43**(3), 030401 (2016). https://doi.org/10.1088/0954-3899/43/3/030401. arXiv:1507.05613
45. A. Abud Abed et al., Low exposure long-baseline neutrino oscillation sensitivity of the DUNE experiment. Phys. Rev. D **105**(7), 072006 (2022). https://doi.org/10.1103/PhysRevD.105.072006. arXiv:2109.01304
46. Y. Kudenko, Hyper-Kamiokande. JINST **15**(07), 07029 (2020). https://doi.org/10.1088/1748-0221/15/07/C07029. arXiv:2005.13641 [physics.ins-det]
47. V. Alenkov et al., Technical design report for the AMoRE $0\nu\beta\beta$ decay search experiment (2015). arXiv:1512.05957
48. S. Rahaman et al., Q value of the Mo-100 double-beta decay. Phys. Lett. B **662**, 111–116 (2008). https://doi.org/10.1016/j.physletb.2008.02.047. arXiv:0712.3337
49. G.B. Kim et al., A CaMoO4 crystal low temperature detector for the AMoRE neutrinoless double beta decay search. Adv. High Energy Phys. **2015**, 817530 (2015). https://doi.org/10.1155/2015/817530. arXiv:1602.07401
50. S.G. Kim et al., A thermal model of low-temperature light detectors for neutrinoless double beta decay experiments. J. Low Temp. Phys. **211**(5-6), 272–280 (2023). https://doi.org/10.1007/s10909-023-02962-6
51. W.T. Kim et al., Optimization of cryogenic calorimetric detection with lithium molybdate crystals for AMoRE-II experiments. JINST **17**(07), 07034 (2022). https://doi.org/10.1088/1748-0221/17/07/P07034
52. H.B. Kim et al., Status and performance of the AMoRE-I experiment on neutrinoless double beta decay. J. Low Temp. Phys. **209**(5-6), 962–970 (2022). https://doi.org/10.1007/s10909-022-02880-z. arXiv:2211.02825
53. K.R. Woo, H.B. Kim, H.L. Kim, Y.H. Kim, D.H. Kwon, D.Y. Lee, H.J. Lee, S.H. Lee, Y.C. Lee, H.S. Lim, An MMC-based temperature control system for a long-term data collection. J. Low Temp. Phys. **209**(5-6), 1218–1225 (2022). https://doi.org/10.1007/s10909-022-02805-w
54. C. Augier et al., Final results on the $0\nu\beta\beta$ decay half-life limit of ^{100}Mo from the CUPID-Mo experiment. Eur. Phys. J. C **82**(11), 1033 (2022). https://doi.org/10.1140/epjc/s10052-022-10942-5. arXiv:2202.08716
55. J.H. Friedman, Greedy function approximation: A gradient boosting machine. Ann. Stat. **29**, 1189 (2001)
56. J.K. Son et al., Growth and development of pure Li2MoO4 crystals for rare event experiment at CUP. JINST **15**(07), 07035 (2020). https://doi.org/10.1088/1748-0221/15/07/C07035. arXiv:2005.06797
57. O. Gileva, J.S. Choe, H.J. Kim, Y.D. Kim, M.H. Lee, H.K. Park, K.A. Shin, Purification and recovery of $^{100}MoO_3$ in crystal production for AMoRE experiment. JINST **15**(07), 07032 (2020). https://doi.org/10.1088/1748-0221/15/07/C07032. arXiv:2005.06463
58. H. Yeon et al., Preparation of low-radioactive high-purity enriched $^{100}MoO_3$ powder for AMoRE-II experiment. Front. in Phys. **11**, 1142136 (2023). https://doi.org/10.3389/fphy.2023.1142136
59. K. Shin, C. Byeon, J. Choe, O. Gileva, Y. Kim, Y. Kim, E. Lee, M.H. Lee, H. Yeon, Selection and purification of Li_2CO_3 precursor for bolometric double beta decay experiments. Front. in Phys. **12**, 1347162 (2024). https://doi.org/10.3389/fphy.2024.1347162
60. C. Lee, H.S. Jo, C.S. Kang, G.B. Kim, I. Kim, S.R. Kim, Y.H. Kim, H.J. Lee, J.H. So, Y.S. Yoon, Vibration isolation system for cryogenic phonon-scintillation calorimeters. JINST **12**(02), 02057 (2017). https://doi.org/10.1088/1748-0221/12/04/A04001
61. H. Prihtiadi et al., Measurement of the cosmic muon annual and diurnal flux variation with the COSINE-100 detector. JCAP **02**, 013 (2021). https://doi.org/10.1088/1475-7516/2021/02/013
62. A. Agrawal et al., Radioassay of the materials for AMoRE-II experiment. Front. in Phys. (in press). https://doi.org/10.3389/fphy.2024.1362209
63. V.V. Alenkov et al., Projected background and sensitivity of AMoRE-II (in prepation)
64. Y. Oh, AMoRE-II preparation status. PoS **TAUP2023**, 214 (2024). https://doi.org/10.22323/1.441.0214
65. J. Engel, J. Menéndez, Status and future of nuclear matrix elements for neutrinoless double-beta decay: A review. Rept. Prog. Phys. **80**(4), 046301 (2017). https://doi.org/10.1088/1361-6633/aa5bc5. arXiv:1610.06548

66. R. Bernabei et al., Searching for WIMPs by the annual modulation signature. Phys. Lett. B **424**, 195–201 (1998). https://doi.org/10.1016/S0370-2693(98)00172-5
67. R. Bernabei et al., Dark matter search. Riv. Nuovo Cim. **26N1**, 1–73 (2003)
68. R. Bernabei et al., Final model independent result of DAMA/LIBRA-phase1. Eur. Phys. J. C **73**, 2648 (2013). https://doi.org/10.1140/epjc/s10052-013-2648-7
69. R. Bernabei et al., First model independent results from DAMA/LIBRA-phase2. Nucl. Phys. Atom. Energy **19**(4), 307–325 (2018). https://doi.org/10.15407/jnpae2018.04.307
70. R. Bernabei et al., Further results from DAMA/Libra-phase2 and perspectives. Nucl. Phys. Atom. Energy **22**(4), 329–342 (2021). https://doi.org/10.15407/jnpae2021.04.329
71. C. Savage, G. Gelmini, P. Gondolo, K. Freese, Compatibility of DAMA/LIBRA dark matter detection with other searches. JCAP **0904**, 010 (2009). https://doi.org/10.1088/1475-7516/2009/04/010
72. Y.J. Ko et al., Comparison between DAMA/LIBRA and COSINE-100 in the light of quenching factors. JCAP **11**, 008 (2019). https://doi.org/10.1088/1475-7516/2019/11/008. arXiv:1907.04963
73. K.W. Kim et al., Tests on NaI(Tl) crystals for WIMP search at the Yangyang Underground Laboratory. Astropart. Phys. **62**, 249 (2015). https://doi.org/10.1016/j.astropartphys.2014.10.004. arXiv:1407.1586
74. K. Fushimi et al., Dark matter search project PICO-LON. J. Phys. Conf. Ser. **718**(4), 042022 (2016). https://doi.org/10.1088/1742-6596/718/4/042022
75. G. Adhikari et al., Initial performance of the COSINE-100 experiment. Eur. Phys. J. C **78**(2), 107 (2018). https://doi.org/10.1140/epjc/s10052-018-5590-x
76. I. Coarasa et al., ANAIS-112 sensitivity in the search for dark matter annual modulation. Eur. Phys. J. C **79**(3), 233 (2019). https://doi.org/10.1140/epjc/s10052-019-6733-4. arXiv:1812.02000
77. M. Antonello et al., The SABRE project and the SABRE proof-of-principle. Eur. Phys. J. C **79**(4), 363 (2019). https://doi.org/10.1140/epjc/s10052-019-6860-y. arXiv:1806.09340
78. G. Angloher et al., Results from the first cryogenic NaI detector for the COSINUS project. JINST **12**(11), 11007 (2017). https://doi.org/10.1088/1748-0221/12/11/P11007
79. J. Amaré et al., Performance of ANAIS-112 experiment after the first year of data taking. Eur. Phys. J. C **79**(3), 228 (2019). https://doi.org/10.1140/epjc/s10052-019-6697-4. arXiv:1812.01472
80. G. Adhikari et al., Search for a dark matter-induced annual modulation signal in NaI(Tl) with the COSINE-100 experiment. Phys. Rev. Lett. **123**(3), 031302 (2019). https://doi.org/10.1103/PhysRevLett.123.031302. arXiv:1903.10098
81. G. Adhikari et al., Three-year annual modulation search with COSINE-100. Phys. Rev. D **106**(5), 052005 (2022). https://doi.org/10.1103/PhysRevD.106.052005
82. G. Adhikari et al., Strong constraints from COSINE-100 on the DAMA dark matter results using the same sodium iodide target. Sci. Adv. **7**(46), 2699 (2021). https://doi.org/10.1126/sciadv.abk2699
83. J. Amaré et al., First results on dark matter annual modulation from the ANAIS-112 experiment. Phys. Rev. Lett. **123**(3), 031301 (2019). https://doi.org/10.1103/PhysRevLett.123.031301. arXiv:1903.03973
84. J. Amare et al., Annual modulation results from three-year exposure of ANAIS-112. Phys. Rev. D **103**(10), 102005 (2021). https://doi.org/10.1103/PhysRevD.103.102005. arXiv:2103.01175
85. P. Adhikari et al., Background model for the NaI(Tl) crystals in COSINE-100. Eur. Phys. J. C **78**, 490 (2018). https://doi.org/10.1140/epjc/s10052-018-5970-2
86. J. Amare et al., Analysis of backgrounds for the ANAIS-112 dark matter experiment. Eur. Phys. J. C **79**(5), 412 (2019). https://doi.org/10.1140/epjc/s10052-019-6911-4. arXiv:1812.01377
87. G. Adhikari et al., Background modeling for dark matter search with 1.7 years of COSINE-100 data. Eur. Phys. J. C **81**, 837 (2021). https://doi.org/10.1140/epjc/s10052-021-09564-0
88. M. Antonello et al., Characterization of SABRE crystal NaI-33 with direct underground counting. Eur. Phys. J. C **81**(4), 299 (2021). https://doi.org/10.1140/epjc/s10052-021-09098-5. arXiv:2012.02610
89. B.J. Park et al., Development of ultra-pure NaI(Tl) detectors for the COSINE-200 experiment. Eur. Phys. J. C **80**(9), 814 (2020). https://doi.org/10.1140/epjc/s10052-020-8386-8. arXiv:2004.06287
90. K. Fushimi et al., Development of highly radiopure NaI(Tl) scintillator for PICOLON dark matter search project. PTEP **2021**(4), 043–01 (2021). https://doi.org/10.1093/ptep/ptab020. arXiv:2101.00759
91. H. Lee et al., Performance of an ultra-pure NaI(Tl) detector produced by an indigenously-developed purification method and crystal growth for the COSINE-200 experiment. Front. in Phys. **11**, 1142765 (2023). https://doi.org/10.3389/fphy.2023.1142765. arXiv:2301.04884
92. G. Adhikari et al., An induced annual modulation signature in COSINE-100 data by DAMA/LIBRA's analysis method. Sci. Rep. **13**(1), 4676 (2023). https://doi.org/10.1038/s41598-023-31688-4. arXiv:2208.05158
93. G. Adhikari et al., Search for inelastic WIMP-iodine scattering with COSINE-100. Phys. Rev. D **108**(9), 092006 (2023). https://doi.org/10.1103/PhysRevD.108.092006. arXiv:2307.09814
94. G. Adhikari et al., Search for bosonic super-weakly interacting massive particles at COSINE-100. Phys. Rev. D **108**(4), 041301 (2023). https://doi.org/10.1103/PhysRevD.108.L041301. arXiv:2304.01460
95. Y.J. Ko, H. Park, Remarks on bosonic super-WIMP search experiments. Phys. Rev. D **104**(8), 083030 (2021). https://doi.org/10.1103/PhysRevD.104.083030. arXiv:2105.11109
96. M. Agostini et al., First search for bosonic superweakly interacting massive particles with masses up to 1 MeV/c^2 with GERDA. Phys. Rev. Lett. **125**(1), 011801 (2020). https://doi.org/10.1103/PhysRevLett.125.011801. arXiv:2005.14184
97. C. Ha et al., First direct search for inelastic boosted dark matter with COSINE-100. Phys. Rev. Lett. **122**(13), 131802 (2019). https://doi.org/10.1103/PhysRevLett.122.131802
98. G. Adhikari et al., Search for boosted dark matter in COSINE-100. Phys. Rev. Lett. **131**(20), 201802 (2023). https://doi.org/10.1103/PhysRevLett.131.201802. arXiv:2306.00322
99. G. Adhikari et al., Search for solar bosonic dark matter annual modulation with COSINE-100. Phys. Rev. D **107**(12), 122004 (2023). https://doi.org/10.1103/PhysRevD.107.122004. arXiv:2302.10267
100. J.J. Choi, B.J. Park, C. Ha, K.W. Kim, S.K. Kim, Y.D. Kim, Y.J. Ko, H.S. Lee, S.H. Lee, S.L. Olsen, Improving the light collection using a new NaI(Tl) crystal encapsulation. Nucl. Instrum. Meth. A **981**, 164556 (2020). https://doi.org/10.1016/j.nima.2020.164556. arXiv:2006.02573
101. S.H. Lee, G.S. Kim, H.J. Kim, K.W. Kim, J.Y. Lee, H.S. Lee, Study on NaI(Tl) crystal at −35 °C for dark matter detection. Astropart. Phys. **141**, 102709 (2022). https://doi.org/10.1016/j.astropartphys.2022.102709. arXiv:2111.03328
102. J.J. Choi et al., Exploring coherent elastic neutrino-nucleus scattering using reactor electron antineutrinos in the NEON experiment. Eur. Phys. J. C **83**(3), 226 (2023). https://doi.org/10.1140/epjc/s10052-023-11352-x. arXiv:2204.06318
103. Y.J. Ko, H.S. Lee, Sensitivities for coherent elastic scattering of solar and supernova neutrinos with future NaI(Tl) dark matter search detectors of COSINE-200/1T. Astropart. Phys. **153**, 102890 (2023). https://doi.org/10.1016/j.astropartphys.2023.102890. arXiv:2210.01386
104. K. Shin, O. Gileva, Y. Kim, H.S. Lee, H. Park, Reduction of the radioactivity in sodium iodide (NaI) powder by recrystallization method. J. Radioanal. Nucl. Chem. **317**(3), 1329–1332 (2018). https://doi.org/10.1007/s10967-018-6006-y
105. K. Shin, J. Choe, O. Gileva, A. Iltis, Y. Kim, C. Lee, H.S. Lee, M.H. Lee, H.K. Park, A facility for mass production of ultra-pure NaI powder for the COSINE-200 experiment. JINST **15**(07), 07031 (2020). https://doi.org/10.1088/1748-0221/15/07/C07031. arXiv:2004.13280
106. K. Shin, J. Choe, O. Gileva, A. Iltis, Y. Kim, Y. Kim, C. Lee, E. Lee, H. Lee, M.H. Lee, Mass production of ultra-pure NaI powder for COSINE-200. Front. in Phys. **11**, 1142849 (2023). https://doi.org/10.3389/fphy.2023.1142849. arXiv:2301.05400
107. G. Adhikari et al., Searching for low-mass dark matter via the Migdal effect in COSINE-100. Phys. Rev. D **105**(4), 042006 (2022). https://doi.org/10.1103/PhysRevD.105.042006
108. S. Schoppmann, Review of novel approaches to organic liquid scintillators in neutrino physics. Symmetry **15**(1), 11 (2023). https://doi.org/10.3390/sym15010011. arXiv:2212.11341

109. Y.J. Ko et al., Sterile neutrino search at the NEOS experiment. Phys. Rev. Lett. **118**(12), 121802 (2017). https://doi.org/10.1103/PhysRevLett.118.121802. arXiv:1610.05134
110. S.H. Seo, Y.D. Kim, Dark photon search at Yemilab, Korea. JHEP **04**, 135 (2021). https://doi.org/10.1007/JHEP04(2021)135. arXiv:2009.11155
111. A. Bungau et al., Proposal for an electron antineutrino disappearance search using high-rate ^{8}Li production and decay. Phys. Rev. Lett. **109**, 141802 (2012). https://doi.org/10.1103/PhysRevLett.109.141802. arXiv:1205.4419
112. G. Bellini et al., SOX: Short distance neutrino Oscillations with BoreXino. JHEP **08**, 038 (2013). https://doi.org/10.1007/JHEP08(2013)038. arXiv:1304.7721
113. V. Albanese et al., The SNO+ experiment. JINST **16**(08), 08059 (2021). https://doi.org/10.1088/1748-0221/16/08/P08059. arXiv:2104.11687
114. X.-J. Xu, Z. Wang, S. Chen, Solar neutrino physics. Prog. Part. Nucl. Phys. **131**, 104043 (2023). https://doi.org/10.1016/j.ppnp.2023.104043. arXiv:2209.14832
115. M. Agostini et al., Comprehensive measurement of *pp*-chain solar neutrinos. Nature **562**(7728), 505–510 (2018). https://doi.org/10.1038/s41586-018-0624-y
116. J.D. Bjorken, S. Ecklund, W.R. Nelson, A. Abashian, C. Church, B. Lu, L.W. Mo, T.A. Nunamaker, P. Rassmann, Search for neutral metastable penetrating particles produced in the SLAC beam dump. Phys. Rev. D **38**, 3375 (1988). https://doi.org/10.1103/PhysRevD.38.3375
117. B. Batell, R. Essig, Z. Surujon, Strong constraints on Sub-GeV dark sectors from SLAC beam dump E137. Phys. Rev. Lett. **113**(17), 171802 (2014). https://doi.org/10.1103/PhysRevLett.113.171802. arXiv:1406.2698
118. J. Beacham et al., Physics beyond colliders at CERN: Beyond the Standard Model working group report. J. Phys. G **47**(1), 010501 (2020). https://doi.org/10.1088/1361-6471/ab4cd2. arXiv:1901.09966
119. A. Filippi, M. De Napoli, Searching in the dark: the hunt for the dark photon. Rev. Phys. **5**, 100042 (2020). https://doi.org/10.1016/j.revip.2020.100042. arXiv:2006.04640
120. Y.-S. Liu, G.A. Miller, Validity of the Weizsäcker-Williams approximation and the analysis of beam dump experiments: Production of an axion, a dark photon, or a new axial-vector boson. Phys. Rev. D **96**(1), 016004 (2017). https://doi.org/10.1103/PhysRevD.96.016004. arXiv:1705.01633
121. B. Dasgupta, J. Kopp, Sterile neutrinos. Phys. Rept. **928**, 1–63 (2021). https://doi.org/10.1016/j.physrep.2021.06.002. arXiv:2106.05913
122. J.R. Alonso et al., IsoDAR@Yemilab: A conceptual design report for the deployment of the isotope decay-at-rest experiment in Korea's new underground laboratory, Yemilab (2021). arXiv:2110.10635
123. J.R. Alonso et al., IsoDAR@Yemilab: A report on the technology, capabilities, and deployment. JINST **17**(09), 09042 (2022). https://doi.org/10.1088/1748-0221/17/09/P09042. arXiv:2201.10040
124. J. Alonso et al., Neutrino physics opportunities with the IsoDAR source at Yemilab. Phys. Rev. D **105**(5), 052009 (2022). https://doi.org/10.1103/PhysRevD.105.052009. arXiv:2111.09480
125. A.J. Krasznahorkay et al., Observation of anomalous internal pair creation in Be8 : A possible indication of a light, neutral boson. Phys. Rev. Lett. **116**(4), 042501 (2016). https://doi.org/10.1103/PhysRevLett.116.042501, arXiv:1504.01527

Publisher's Note